Liquid-phase exfoliation of F-diamane-like nanosheets

Xianjue Chen, Marc Dubois, Silvana Radescu, Aditya Rawal, Chuan Zhao

Liquid-Phase Exfoliation of F-Diamane-Like Nanosheets

Xianjue Chen [a,*], Marc Dubois [b,*], Silvana Radescu [c], Aditya Rawal [d], Chuan Zhao [a]

[a]School of Chemistry, The University of New South Wales, Sydney, New South Wales 2052, Australia

[b]Université Clermont Auvergne, SIGMA Clermont, CNRS, Institut de Chimie de Clermont-Ferrand (UMR 6296), BP 10448, F-63000, Clermont-Ferrand, France

[c]Departamento de Física, Universidad de La Laguna, Instituto de Materiales y Nanotecnología, 38200 La Laguna S/C Tenerife, Spain

[d]Mark Wainwright Analytical Centre, University of New South Wales, Sydney, New South Wales 2052, Australia

*Corresponding authors.

E-mails: xianjue.chen@unsw.edu.au (Xianjue Chen); marc.dubois@uca.fr (Marc Dubois)

Highlights

- Poly(dicarbon monofluoride) $(C_2F)_n$ was synthesized by the fluorination of graphite.
- The $(C_2F)_n$ is essentially made of stacked layers of "F-diamane".
- Liquid-phase exfoliation of $(C_2F)_n$ yielded ultrathin nanosheets.
- The "F-diamane"-like structure was retained after exfoliation.
- Density functional theory calculations support the experimental results.

Abstract

Fluorinated single-layer diamond ("F-diamond") is a new form of two-dimensional (2D) carbon allotrope. Herein, poly(dicarbon monofluoride) $(C_2F)_n$ which is essentially made of stacked layers of "F-diamane" has been synthesized and exfoliated in a variety of solvents to yield well-dispersed ultrathin sheets. Microscopic and spectroscopic analyses revealed that the exfoliated nanosheets retained the "F-diamane"-like structure. The experimental results are also supported by density functional theory (DFT) calculations.

Keywords: diamane, graphite fluoride, fluorination, exfoliation, 2D materials

1. Introduction

Atomically thin diamond ("diamane") has recently emerged as a new two-dimensional carbon allotrope. Theoretical studies first predicted the conversion of AB-stacked few-layer graphene into diamane films through sufficient formation of carbon-fluorine (C-F) or carbon-hydrogen (C-H) bonds on the two free surfaces [1-4]. Odkhuu et al. showed that when a one-side surface of a bilayer graphene grown on a transition metal surface was fluorinated, the energetics for the conversion to sp^3-bonded films were significantly lower than that for the free-standing bilayer [5]. Fluorination and hydrogenation of graphene have been experimentally investigated [6,7]. Recent advances in chemical vapor deposition (CVD) growth of graphene towards precise quality control (number of layers, crystallinity, coverage and uniformity) have indicated pathways for converting few layers of graphene into "diamane" films [8]. Bakharev et al. [9] first demonstrated that fluorine chemisorption on CVD-grown, AB-stacked, bilayer graphene led to a fluorinated diamond monolayer ("F-diamane"). Rajasekaran et al. [10] reported experimental evidence that hydrogen adsorption could induce partial phase transition of few-layer graphene to an sp^3-bonded structure on a Pt(111) surface. Diamane-like structures have also been achieved by compressing trilayer graphene to ultrahigh-pressure (>20 GPa) at room temperature [11], or exposing bilayer graphene to hydrogen radicals generated by a hot filament process [12]. The stability, mechanical, electronic, optical and thermal properties of diamane structures stabilized with H, F or Cl atoms have been predicted using DFT simulations [13,14].

Fluorination of graphite was first reported in 1934, where graphite was exposed to fluorine gas at moderate temperatures (400-600 °C) [15]. The product is a solid fluorocarbon compound that has been loosely classified as a graphite intercalation compound due to its layered structures derived from graphite [16]. By controlling the fluorination process, two forms of graphite fluoride can be obtained: "Stage-1" $(CF)_n$, fluorine atoms are bonded above and under graphene planes, where every carbon atom is covalently bonded with a fluorine atom, producing a chair-type structure; "Stage-2" $(C_2F)_n$, fluorine atoms are inserted into every second layer of graphite where the carbon atoms establish an sp^3 orbital with a double-decked structure. The structural model proposed in previous studies [17-19] is illustrated in **Fig. 1**a, b. Note that the $(C_2F)_n$ is essentially composed of stacked layers of "F-diamane". The low surface energy caused by the short, strong C-F bonds results in a low friction coefficient between the layers [20], and thus the "F-diamane" layers could be exfoliated under shear.

Liquid-phase exfoliation has been widely used in the preparation of single-layer and few-layer platelets from bulk flakes of layered materials including graphite, hexagonal boron nitride, black phosphorus, transition metal dichalcogenides, and more [21-24]. In the case of $(CF)_n$, many different "top-down" exfoliation methods have been developed [25-31]. Unlike the CVD technique that has a tight process control and a relatively high cost, liquid-phase exfoliation is a simple, versatile means to produce ultrathin layers in large quantities [32]. Herein, we show sonication-assisted exfoliation of $(C_2F)_n$ in solvents yields few-layer platelets with an "F-diamane"-like structure.

2. Material and Methods

2.1 Preparation of materials

Poly(dicarbon monofluoride) $(C_2F)_n$ was synthesized using the conventional method. A monel boat containing Madagascar natural graphite was placed in a nickel reactor and heated to 350 °C under pure F_2 gas flow for 8 h. $(CF)_n$ (GT1FF012) were purchased from ACS Material and used without further modification. Suspensions (10 mL) of $(C_2F)_n$ (0.5 mg mL^{-1}) in water or organic solvents were subject to sonication using a probe-sonicator (Branson Digital Sonifier 450; 20% amplitude, 1h; under ice bath and with a pulse effect of 10s on and 10s off to avoid overheating). The suspensions in organic solvents were centrifuged (Centrifuge 5810, Eppendorf, 117 × *g*, 10 min) to remove non-dispersible species. The supernatants were separated affording stable suspensions.

2.2 Material characterization

XRD patterns were obtained using a PANalytical Xpert Multipurpose X-ray Diffraction System and analyzed using X'Pert HighScore Plus software. SEM images were recorded on a FEI Nova NanoSEM 450 FE-SEM. XPS spectra were acquired using an ESCALAB 250 Xi, Thermo Scientific. The ^{19}F solid-state NMR spectra were acquired on a Bruker AVANCE III 700 MHz spectrometer with a 16.4 tesla superconducting magnet, operating at a frequency of 658.88 MHz for the ^{19}F nucleus. Approximately 30 mg of sample was packed in a in 3.2 mm zirconia rotors fitted with Vespel® caps and spun to 24 kHz at the magic angle in a double resonance 3.2 mm HX Low-gamma MAS probehead. The ^{19}F 90° pulse length of 2.5 μs was used with sufficient recycle delay to ensure full signal relaxation. The ^{19}F chemical shifts were referenced to $CFCl_3$ at

0 ppm using the ^{19}F signal of polytetrafluoroethylene (PTFE) at -122.7 ppm as a secondary reference. The DMFIT software was used for deconvolution of the NMR spectra [33]. AFM images were acquired on a Bruker Dimension ICON SPM operating in the tapping mode. A dispersion of $(C_2F)_n$ in chloroform was drop-cast onto a freshly cleaved mica substrate and dried in air. AFM images were analyzed using the Gwyddion SPM software. TEM specimens were prepared by drop casting a $(C_2F)_n$ dispersion onto a holey carbon-coated Cu grid (SPI Supplies, #2450-AB) and dried in air. TEM/STEM analysis was performed using a JEOL JEM-F200 Multi-Purpose FEG-S/TEM operating at an accelerating voltage of 80 kV. Image J and Pathfinder were used for processing the TEM and elemental mapping images. Raman spectra were recorded on a Renishaw InVia 2 Raman spectrometer at room temperature with a 532 nm laser excitation. For FTIR, pellets were prepared by compressing the well-mixed KBr and sample powders. FTIR was recorded on a Spectrum 100/Spotlight 400 spectrometer in the transmission mode.

2.3 Computational details

The DFT calculations for the (C_2F) monolayer were performed using the Vienna Ab Initio Simulation Package (VASP) computational code, which implements the projector-augmented wave method (PAW), and the Perdew-Burke-Ernzerhof (PBE) form of the generalized gradient approximation that was taken for the exchange and correlation (XC) energy [34-37]. The PBEsol approach was also used, and the structural results are similar when compared to the PBE method (Table S1 in the Supporting Information). A large vacuum space between monolayers of 33.5 Å is set to avoid interaction between the periodic images of the layers. In the ab initio calculations, only the two 2s and two 2p outermost valence electrons of C, and the two 2s and five 2p outermost valence electrons of F were explicitly taken into account, the rest of the electrons are considered frozen at the core. To ensure a convergence in the energy differences between phases of around 1 meV we used dense uniform 15x15x1 k-points Monkhorst-Pack grids to sample the Brillouin zone, and a cutoff in the kinetic energy of the plane-waves basis set of 600 eV. To obtain the unstrained configuration, the atomic positions and lattice vectors were fully relaxed (with residual forces less than 0.005 eV $Å^{-1}$) and the optimized (relaxed) coordinates were then used for the electronic, elastic, vibrational properties, and core level binding energies.

The mechanical stability of the unstrained monolayer was checked in terms of elastic constants (Born stability criteria). In VASP calculations, the elastic constants for 2D materials can be obtained by normalizing the calculated constant with the lattice parameter c. By applying a set of suitable deformations to the monolayer and taking into account the reduced dimensionality, we obtained the in-plane elastic constants, where the Young's modulus (E) and Poisson's ratio (ν) can be obtained from the following relationships [38]:

$$E = (C_{11}^2 - C_{12}^2)/C_{11} \qquad \upsilon = \frac{C_{12}}{C_{11}}$$

To check the stability of 2D-(C_2F) we have calculated the phonon dispersion curves in the whole BZ zone (a structure is locally stable only if the calculated frequencies of all its phonon modes are positive; otherwise, the presence of negative (imaginary) frequencies indicates an instability). To calculate the phonons we used the density functional perturbation theory (DFPT) as implemented in the VASP code and a post processing Phonopy package to analyze the vibrational modes [39].

The electron localization function (ELF) was calculated from the valence electronic density obtained within the PAW scheme implemented in VASP (where the core electrons are considered frozen and not explicitly considered). The visualization of the ELF isosurface was done with VESTA 3.5.5 [40]. We further performed a topological analysis of the all-electron density (the sum of the core and valence densities) calculated with VASP by means of the quantum theory of atoms in molecules (QTAIM), using the CRITIC2 code [41,42]. For the calculation of the core level binding energies of the C1s and F1s core states with a half core-hole effects, we have applied the so-called final state method based in DFT [43].

3. Results and Discussion

The synthesis of poly(dicarbon monofluoride) $(C_2F)_n$ was first reported in 1979 [17]. The yield of $(C_2F)_n$ depends on a number of factors, including the crystallinity of raw carbon, the fluorinating reagent, and the reaction temperature. Herein, $(C_2F)_n$ was synthesized by heating graphite flakes to 350 °C under pure F_2 gas flow (dynamic mode). SEM image shows the $(C_2F)_n$ flakes range from 5-20 μm in size, **Fig. 1**c. The X-ray diffraction (XRD) pattern, **Fig. 1**d, suggests an interlayer distance of ~0.81 nm corresponding to the (001) diffraction line of $(C_2F)_n$. The peak at 42.1° is assigned to the (100) reflection (d = 0.21 nm). These values are in good agreement with the proposed structural model. The key distinguishing feature for $(C_2F)_n$

compared to $(CF)_n$ is that the "stage-2" intercalated structure has a larger interlayer distance. The XRD pattern (**Fig. S1**b) for $(CF)_n$ suggests an interlayer distance of 0.64 nm. The relatively broad peaks for the (001) and (100) reflections suggests a high degree of structural disorder in $(C_2F)_n$ and $(CF)_n$. A peak at 26.6° observed for both $(C_2F)_n$ and $(CF)_n$ corresponds to the (002) diffraction from residual non-fluorinated graphitic structure.

The surface composition and C-F bonding of $(C_2F)_n$ was investigated using X-ray photoelectron spectroscopy (XPS). The survey spectrum (**Fig. 2**a) collected from $(C_2F)_n$ shows that the composition is mainly C (60.2 at.%) and F (36.7 at.%). The difference in the fluorine-to-carbon (F/C) ratio ($CF_{0.61}$ vs. $CF_{0.5}$) could be owing to the presence of structural defects that allow carbon to be terminated with fluorine by forming CF_2 and CF_3 groups on the edges of the layers, and/or the presence of a small amount of $(CF)_n$ [17]. The XPS result for $(CF)_n$ (**Fig. S1**c) shows a significantly higher F/C ratio of 1.0.

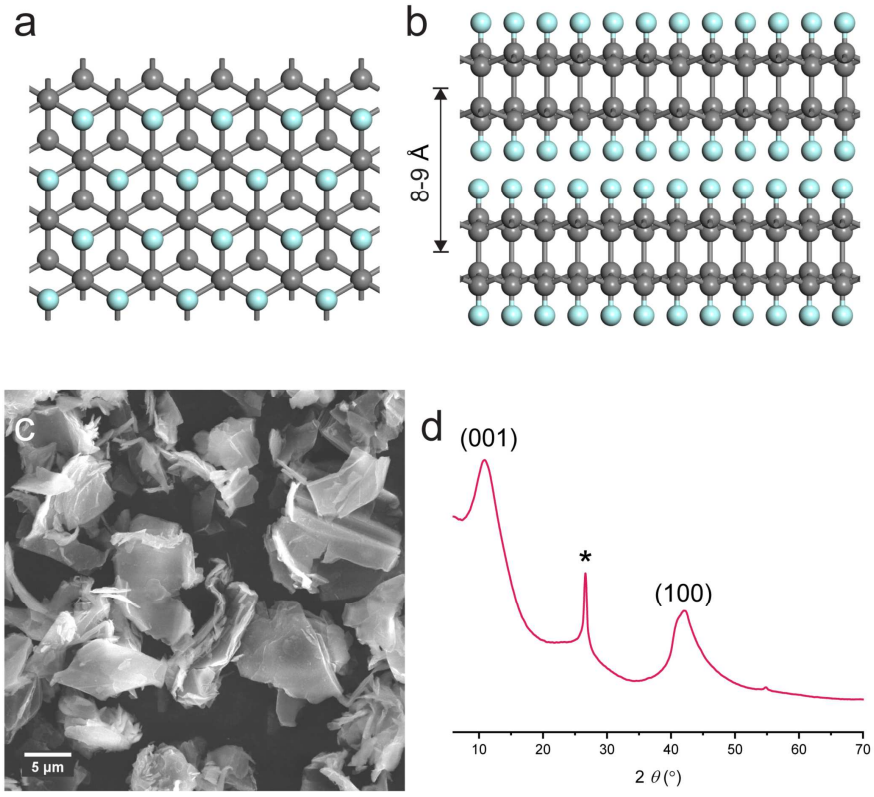

Fig. 1 The proposed (a) top-view and (b) side-view crystal structure of $(C_2F)_n$. (c) SEM image and (d) XRD pattern of $(C_2F)_n$ flakes. The "*" symbols refer to the (002) diffraction from residual graphitic structure.

The high electronegativity of fluorine induces strong chemical shifts in the C1s binding energy, **Fig. 2**b. The C1 peak at 284.7 eV is associated with the carbon atoms in the sp^2- and/or sp^3-bonded structures; C2 (285.7 eV) and C3 (288.0 eV) peaks can be assigned to non-fluorinated carbons linked to fluorine bound carbons (C-CF and CF-C-CF species); C4 peak (289.7 eV) corresponds to the carbons forming C-F bonds; C5 peak (291.6 eV) is assigned to CF_2 groups that exist in the periphery of amorphous regions and/or platelet edges [44]. **Fig. S1**d shows the C1s spectra of $(CF)_n$, where the C1, C2, and C3 peaks have much lower relative intensities. This suggests that each fluorinated carbon in $(CF)_n$ is predominantly bound to three other fluorinated carbons. The F1s peak (**Fig. 2**b and **S1**d) at 688.2 eV is associated with covalently bound fluorine in both $(C_2F)_n$ and $(CF)_n$.

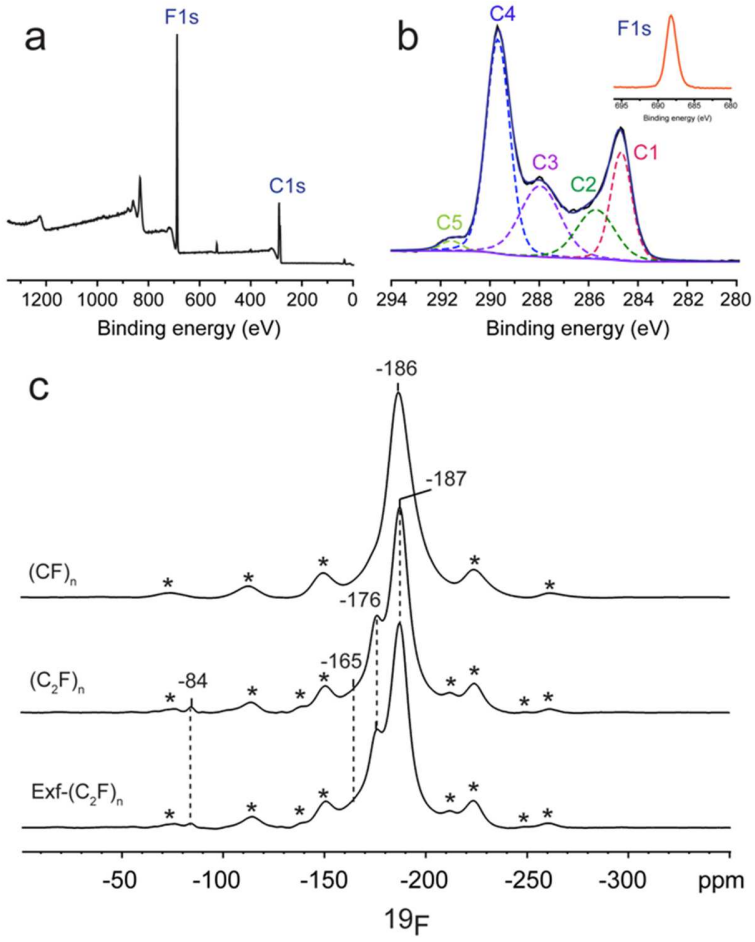

Fig. 2 XPS (a) survey and (b) C1s and F1s spectra for $(C_2F)_n$. (c) ^{19}F Solid state NMR of $(CF)_n$, $(C_2F)_n$, and exfoliated $(C_2F)_n$.

Exfoliation of $(C_2F)_n$ within various solvents (water, ethanol, toluene, chloroform, and DMF) was carried out using probe sonication, **Fig. S2**. $(C_2F)_n$ can hardly be dispersed in water due to its hydrophobic nature, and most of the exfoliated material was floating on the water surface or sank to the bottom. Exfoliation within ethanol, chloroform, or DMF resulted in homogenous suspensions after removing any non-dispersible species using centrifugation. The Tyndall effect was observed for all the solvents (including water), suggesting the formation of colloidal dispersions of exfoliated $(C_2F)_n$. XPS spectra (**Fig. S3**) of the exfoliated $(C_2F)_n$ show increased F/C ratios, 0.90, 0.85, 0.80, 0.82 and 0.90 for water, ethanol, toluene, chloroform and DMF, respectively. This could be owing to the exfoliation-induced fragmentation of $(C_2F)_n$ that exposes more edges where CF_2 and CF_3 groups are present, and/or conversion of $(C_2F)_n$ surface into $(CF)_n$ due to partial defluorination.

Raman spectroscopy and Fourier-transform infrared spectroscopy (FTIR) analyses were carried out for $(CF)_n$, $(C_2F)_n$, and exfoliated $(C_2F)_n$, as shown in **Fig. S1** and **S4**. For $(CF)_n$, the Raman activity was quenched due to its wide band gap [31], whereas for $(C_2F)_n$ the Raman bands associated with carbon D (1324 cm^{-1}) and G (1586 cm^{-1}) bands were observed, which are close to the values measured in previous studies [45]. In FTIR spectra, the strongest bands at 1192 cm^{-1} for $(CF)_n$ and 1222 cm^{-1} for $(C_2F)_n$ can be assigned to the C-F stretching vibration of tertiary carbon atoms [46]. A medium band at 1348 cm^{-1} was observed in the spectra, possibly corresponding to asymmetric stretching vibrations of peripheral CF_2 groups [47]. The exfoliated $(C_2F)_n$ show similar Raman and FTIR features to $(C_2F)_n$, which suggests that the "F-diamane" structure was retained.

Fig. 2c shows the ^{19}F solid state NMR spectra of $(CF)_n$, $(C_2F)_n$, and exfoliated $(C_2F)_n$. The presence of covalent C-F bonding in $(C_2F)_n$ and $(CF)_n$ is confirmed by the position of the isotropic ^{19}F NMR peaks. The primary signal of the ^{19}F species was observed at the chemical shifts of -186 ppm and -187 ppm (vs $CFCl_3$), for $(CF)_n$ and $(C_2F)_n$ respectively. The $(C_2F)_n$ and the exfoliated $(C_2F)_n$ showed nearly identical ^{19}F spectra, indicating that the exfoliation process did not induce major chemical changes in the material. A relatively weak signal at -84 ppm was observed for $(C_2F)_n$, corresponding to terminal CF_3 groups. An associated isotropic signal relating to CF_2 groups at -120 ppm is also expected [48,49], but in the present case is overlapped by spinning sidebands. A resolved shoulder at -176 ppm was observed in the $(C_2F)_n$, while a similar signal albeit with a lower resolution is also evident in $(CF)_n$. This signal is typical of

$(C_2F)_n$ layers [48,49], corresponding to the stacking of F-C(sp^3)-C(sp^3)-F. Note that in the extreme case, such a chemical shift is similar to fluorinated nanodiamonds, i.e. C(sp^3)-C(sp^3)-F, with F being located only on the surface with a low content (-164 ppm) [50]. Interestingly, from the deconvolution of the ^{19}F spectra (**Fig S5**), the $(C_2F)_n$ shows a relatively broad signal near -168 ppm suggesting the formation of such ^{19}F species.

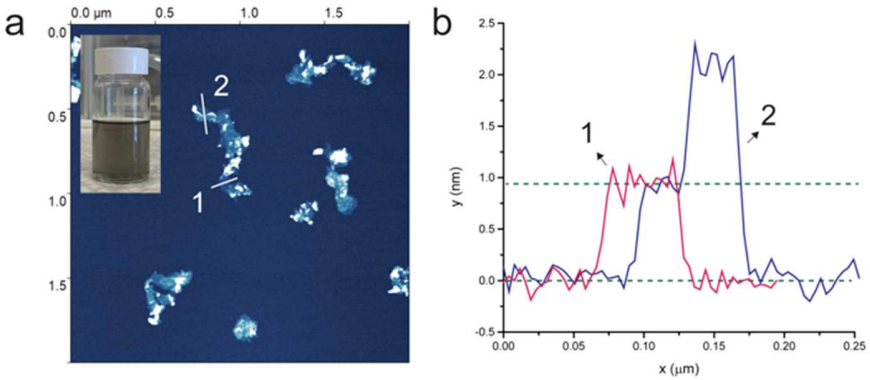

Fig. 3 (a) AFM image of exfoliated $(C_2F)_n$ platelets, with (b) the corresponding height analyses along the lines indicated in (a). A colloidal suspension containing exfoliated $(C_2F)_n$ platelets is shown in the inset.

Atomic force microscope (AFM) was used to examine the size and thickness of the exfoliated $(C_2F)_n$. **Fig. 3**a shows a typical image of the platelets from the chloroform dispersion. The particle size in lateral dimension shows a roughly 100-fold decrease to 50-200 nm, which could result from exfoliation and/or centrifugation that removed larger flakes. AFM height analysis of the exfoliated $(C_2F)_n$ (**Fig. 3**b) suggests a layered structure, with a single layer roughly 0.9 nm in thickness.

Fig. 4a shows a transmission electron microscopy (TEM) image of a typical exfoliated $(C_2F)_n$ nanosheet. The corresponding selected area electron diffraction (SAED) pattern (**Fig. 4**b) has a six-fold symmetry, indicating a hexagonal symmetry for the exfoliated $(C_2F)_n$. Note that the intensities of the first-order diffraction peaks are higher than those of the second-order peaks. This feature is consistent with the reported result for a suspended fluorinated bilayer graphene ("F-diamane"). For bilayer or few-layer graphene, the first-order diffraction peaks have lower intensities than the second-order peaks [9]. A magnified TEM image (**Fig. 4**c), from the indicated area in **Fig. 4**a, shows the edge of the platelet, with a further zoomed-in image in the inset

demonstrating the presence of 2-3 layers. **Fig. 4**d shows a plot of profile along the line in **Fig. 4**c inset, showing an interlayer distance of ~0.9 nm. The interlayer distance ranged from 0.8-0.9 nm along the lattice on the platelet edge. This value is consistent with the XRD and AFM results, and is in good agreement with the proposed model. The high-resolution TEM (HRTEM) image of an exfoliated $(C_2F)_n$ and its corresponding fast Fourier transform (FFT) pattern (**Fig. S6**) suggest a hexagonal crystalline order, which is consistent with the reported result [9]. Elemental maps of carbon and fluorine acquired in scanning transmission electron microscopy (STEM) mode indicate a uniform presence of carbon and fluorine elements in the exfoliated $(C_2F)_n$.

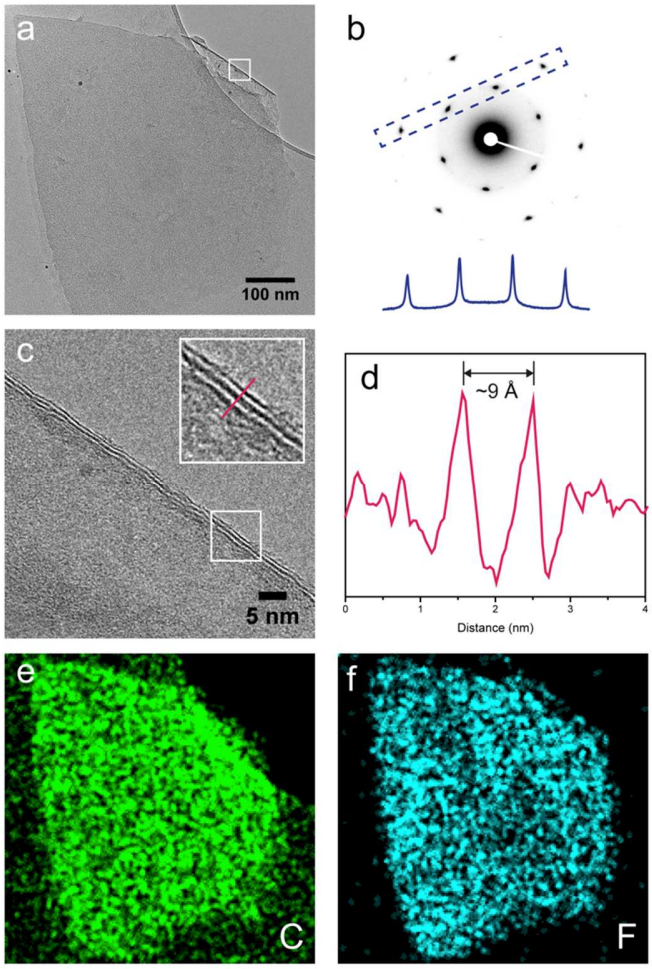

Fig. 4 (a) TEM image of an exfoliated $(C_2F)_n$ platelet, with (b) the corresponding SAED pattern. (c) Magnified TEM image from the indicated area in (a), showing the edge of the platelet. The inset in (c) shows a further magnified image of the edge. (d) A plot of the profile along the line in (c) inset, indicating a ~0.9 nm interlayer distance. (e, f) Elemental maps of C and F from the exfoliated $(C_2F)_n$ platelet.

Fig. S7 shows the core-loss electron energy loss spectroscopy (EELS) spectrum of the exfoliated $(C_2F)_n$. The 1s-π* and 1s-σ* transition peaks can be seen in the C-K edge. Both peaks were observed even for highly fluorinated graphite samples [51,52]. The presence of π* peak could arise from non-fluorinated graphitic species due to the less uniform fluorination of graphite flakes and/or partial defluorination during exfoliation. This is also evident in the XRD and XPS results discussed above. The relatively low intensity of π* peak compared to that of σ* peak indicates the disruption of the conjugated π-orbital network owing to fluorination.

The structure of $(C_2F)_n$ appeared to be sensitive to electron beam irradiation, which is evident when comparing the TEM images (**Fig. S8**) taken from the same area before and after short-term exposure to the electron beam under TEM. Such sensitivity was also observed in a previous study where electron beam induced defluorination to bilayer graphene film [9]. Nevertheless, we found the structure of the exfoliated $(C_2F)_n$ stable after heating up to 300°C in air, as evident by XRD and ^{19}F NMR (**Fig. S9**).

DFT calculations were used to investigate the stability and C-F bonding of an "F-diamane"-like structure, as well as its mechanical and electronic properties. The structure of an unstrained monolayer is shown in **Fig. 5**. The calculated bond lengths and cell parameters for the unstrained (C_2F) monolayer are listed in **Table 1**.

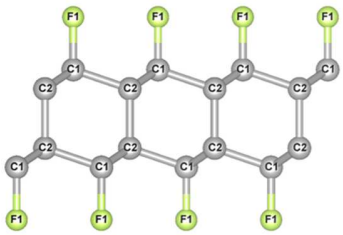

Fig. 5 Crystal structure of a "F-diamane"-like (C_2F) monolayer.

Table 1. Crystallographic description of the equilibrium (C_2F) monolayer.

2D-(C_2F)	Space Group	Atomic Position
V_o = 219.5 Å^3	N°164 *P-3m1*	C1 2d (1/3, 2/3, 0.467)
C2-C2 = 1.554 Å	$a = b$ = 2.559 Å; c =	C2 2c (0.000, 0.000,
C2-C1 = 1.561 Å	38.711 Å	0.520)
C1-F1 = 1.378 Å	α = β = 90.00 γ = 120.00	F1 2d (1/3, 2/3, 0.431)

The results for the elastic stiffness verify the Born's mechanical stability criteria. The calculated values of the in-plane Young's modulus and Poisson's ratio are 478.98 N m^{-1} and 0.10, respectively. Based on the electronic band structure calculation, we found a direct band gap at the Gamma point (4.02 eV, see **Fig. S10**) for the 2D-(C_2F) structure.

The local analysis of the electron density and its Laplacian at bond critical points (BCP) within the framework of the QTAIM method were used to investigate the covalency character of the chemical bonds in this structure. The C-C bonds are characterized by a higher electron density and larger negative Laplacian than the C-F bonds (see **Table 2**) indicating the typical covalent-shared interaction between the two C atoms, as seen from the ELF plots (see **Fig. S11**a). As shown in **Fig. S11**b, the higher electronegativity of fluorine shifts the BCP (along the C(1)-F(1)) path towards the C atom. A BCP was also found along the F(1)-F(1) path, which is characterized by a very small value for both the electron density and the (positive) Laplacian. The C-F bonds with a smaller positive value of the Laplacian are understood to have partial ionic/covalent character.

A phonon dispersion curve of the 2D-(C_2F) structure has been calculated using the DFTP method. As shown in **Fig. 6**, no imaginary frequency appears indicating that the monolayer is stable at ambient conditions.

Table 2. Charge density $\rho(r)$ and its Laplacian $\nabla^2\rho(r)$ calculated at the BCP, in atomic units.

Chemical meaning	**ρ (r)**	**$\nabla^2\rho$ (r)**
C(2) - C(2)	0.2329	-0.5271
C(2) - C(1)	0.2377	-0.5401
C(1) - F(1)	0.2575	0.1259
F (1) - F(1)	0.0148	0.0856

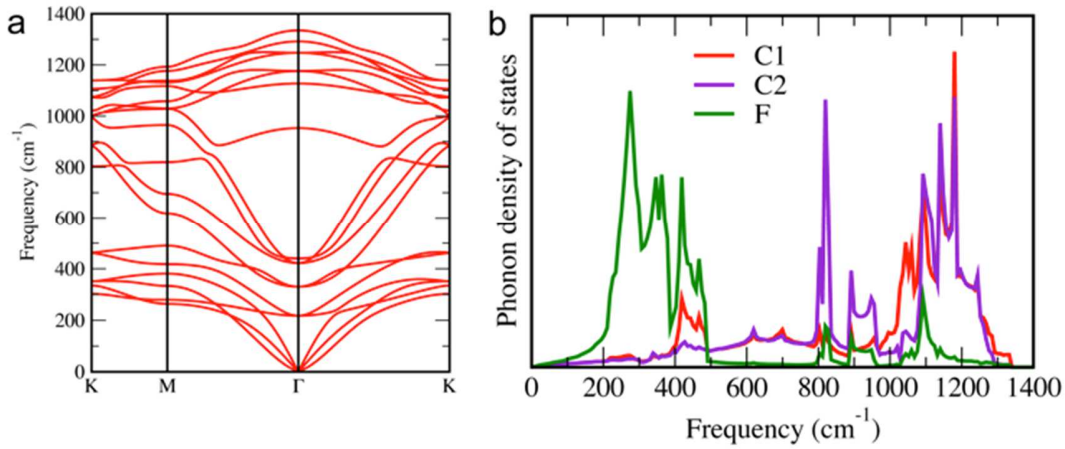

Fig. 6 Phonon dispersion curves of 2D-(C_2F) (a) and vibrational DOS (b).

To complete the study on the vibrational properties, we analyzed the zone-center phonons for the unstrained (C_2F) monolayer, **Table 3**. The mechanical representation yields the following multiplicities for the symmetry of the modes at the zone center: $3A_{1g} + 3A_{2u} + 3E_u + 3E_g$, where the A_{2u} and E_u modes are Infrared and Hyper-Raman active modes, and the A_{1g} and E_g modes are active under Raman. The study of the vibrational properties of the (C_2F) monolayer confirms the experimental results on Raman and FTIR spectroscopy carried out in this work, showing an IR medium band at approximately 1300 cm^{-1}.

In order to interpret the binding energies of the core levels measured by XPS, we performed DFT calculations for the C1s and F1s core states in the final state approximation. The calculated values of the binding energies are given in **Table 4**. From these results we can see that the C atoms are bonded only to other C atoms (C1s-C) as the C-1s values are smaller than the case where they are attached to fluorine (C1s-F), a similar situation previously observed in a study on a C_2F-sp^3 slab supercell [53]. The higher energy values of the core level obtained for the "F-diamane" monolayer can be related to the more covalent character of the C-F bonds than in the slab model (which is also supported by the calculated values of the Laplacian at the BCP). Our DFT results are in fair agreement with the experimental values of the core level.

Table 3. Calculated Raman- and Infrared-active phonon modes.

Active modes	Raman (cm^{-1})	Infrared (cm^{-1})
E_g	216.92, 421.63, 1247.23	-
A_{1g}	440.34, 1127.35, 1292.19	-
E_u	-	329.66, 1176.01
A_{2u}	-	915.07, 1307.17

Table 4. Core level energies obtained in the DFT calculations. The C1s and F1s energy values are referred to the electrostatic potential at vacuum.

Core hole level site	Core level (eV)
C1s (C)	289.1
C1s (F)	290.5
F1s (C)	692.7

4. Conclusions

We have demonstrated a strategy for preparing ultrathin "F-diamane"-like structures by fluorinating graphite to poly(dicarbon monofluoride) $(C_2F)_n$, followed by "top-down" exfoliation of $(C_2F)_n$ in a range of solvents. Different microscopic and spectroscopic analyses have been used to reveal the structure of the exfoliated $(C_2F)_n$ nanosheets. Here we summarize the key experimental evidence for the presence of "F-diamane" structure: (i) The ^{19}F NMR result shows the two types of C-F bonds related to the stacking of F-C(sp^3)-C(sp^3)-F (-176 ppm) and F-C(sp^3)-F (-187 ppm). Both C-F bonds are present regardless the number of layers, and their chemical shifts don't change with this number. This can be used as a direct evidence for the presence of interlayer C-C bonds in the exfoliated $(C_2F)_n$. (ii) The TEM images show a layered structure with an interlayer distance of 0.8-0.9 nm for the exfoliated $(C_2F)_n$, which is consistent with the XRD

and AFM results, and agrees with the proposed $(C_2F)_n$ structural model that is made of stacked layers of "F-diamane". (iii) The SAED and FFT patterns indicate a hexagonal symmetry for the few-layer $(C_2F)_n$, and the intensities of the first-order SAED peaks are higher than those of the second-order peaks. This is consistent with the reported TEM result for "F-diamane" [9]. Here we also suggest that TEM must be used cautiously with specific settings such as low accelerating voltage and short exposure time, as the structure of $(C_2F)_n$ was found to be sensitive to electron beam irradiation, and electron beam could induce defluorination [9]. The calculated topological parameters at the BCP suggested an increasing covalent character of the C-F bonds. This is related to higher energy values obtained for the core level, which is in good agreement with the experimental data. This method is suitable for preparing "F-diamane"-like materials in large quantities. Additionally, larger flakes of $(C_2F)_n$ could be made by fluorination of HOPG or graphite with a larger flake size, which might allow a direct mechanical delamination of "F-diamane" single layers, e.g. using a sticky tape.

Author Contribution

Xianjue Chen: Conceptualization; Data curation; Formal analysis; Funding acquisition; Investigation; Methodology; Project administration; Resources; Validation; Visualization; Writing - original draft; Writing - review & editing. **Marc Dubois:** Conceptualization; Funding acquisition; Methodology; Resources; Validation; Writing - original draft; Writing - review & editing. **Silvana Radescu:** Data curation; Formal analysis; Funding acquisition; Methodology; Resources; Validation; Writing - original draft; Writing - review & editing. **Aditya Rawal:** Formal analysis; Investigation; Writing - original draft; Writing - review & editing. **Chuan Zhao:** Funding acquisition; Resources.

Declaration of competing interest

The authors declare that they have no known competing financial interests, personal relationships or organizations that could inappropriately influence the work reported in this paper.

Acknowledgment

X.C. acknowledges the support from the Australian Research Council (DE180100294). S.R. acknowledges the support from Spanish MICINN Project No. PID2019-106383GB-C43. C.Z. is

grateful for the award of Future Fellowship from the Australian Research Council (FT170100224). The authors thank Xiao Wang for drawing the crystal structure model in Fig. 1. The authors thank the Mark Wainwright Analytical Centre at the University of New South Wales.

References

[1] L.A. Chernozatonskii, P.B. Sorokin, A.G. Kvashnin, D.G. Kvashnin, Diamond-Like C_2H Nanolayer, Diamane: Simulation of the Structure and Properties, JETP Lett. 90 (2009) 134. https://doi.org/10.1134/S0021364009140112.

[2] M.A. Ribas, A.K. Singh, P.B. Sorokin, B.I. Yakobson, Patterning Nanoroads and Quantum Dots on Fluorinated Graphene, Nano Res. 4 (2011) 143. https://doi.org/10.1007/s12274-010-0084-7.

[3] A.G. Kvashnin, L.A. Chernozatonskii, B.I. Yakobson, Phase Diagram of Quasi-Two-Dimensional Carbon, From Graphene to Diamond, Nano Lett. 14 (2014) 676. https://doi.org/10.1021/nl403938g.

[4] L.Y. Antipina, P.B. Sorokin, Converting Chemically Functionalized Few-Layer Graphene to Diamond Films: A Computational Study, J. Phys. Chem. C 119 (2015) 2828. https://doi.org/10.1021/jp510390b.

[5] D. Odkhuu, D. Shin, R.S. Ruoff, N. Park, Conversion of multilayer graphene into continuous ultrathin sp^3-bonded carbon films on metal surfaces, Sci. Rep. 3 (2013) 3276. https://doi.org/10.1038/srep03276.

[6] D.C. Elias, R.R. Nair, T.M.G. Mohiuddin, S.V. Morozov, P. Blake, M.P. Halsall, A.C. Ferrari, D.W. Boukhavlov, M.I. Katsnelson, A.K. Geim, K.S. Novoselov, Control of Graphene's Properties by Reversible Hydrogenation: Evidence for Graphane, Science 323 (2009) 610. https://doi.org/10.1126/science.1167130.

[7] R.R. Nair, W. Ren, R. Jalil, I. Riaz, V.G. Kravets, L. Britnell, P. Blake, F. Schedin, A.S. Mayorov, S. Yuan, M.I. Katsnelson, H.M. Cheng, W. Strupinski, L.G. Bulusheva, A.V. Okotrub, I.V. Grigorieva, A.N. Grigorenko, K.S. Novoselov, A.K. Geim, Fluorographene: A Two-Dimensional Counterpart of Teflon, Small 6 (2010) 2877. https://doi.org/10.1002/smll.201001555.

[8] M. Huang, P.V. Bakharev, Z.J. Wang, M. Biswal, Z. Yang, S. Jin, B. Wang, H.J. Park, Y. Li, D. Qu, Y. Kwon, X. Chen, S.H. Lee, M.G. Willinger, W.J. Yoo, Z. Lee, R.S. Ruoff, Large-Area Single-Crystal AB-Bilayer and ABA-Trilayer Graphene Grown on a Cu/Ni(111) Foil, Nature Nanotechnol. 15 (2020) 289. https://doi.org/10.1038/s41565-019-0622-8.

[9] P.V. Bakharev, M. Huang, M. Saxena, S.W. Lee, S.H. Joo, S.O. Park, J. Dong, D.C. Camacho-Mojica, S. Jin, Y. Kwon, M. Biswal, F. Ding, S.K. Kwak, Z. Lee, R.S. Ruoff, Chemically Induced Transformation of Chemical Vapour Deposition Grown Bilayer Graphene into Fluorinated Single-Layer Diamond, Nature Nanotechnol. 15 (2020) 59. https://doi.org/10.1038/s41565-019-0582-z.

[10] S. Rajasekaran, F. Abild-Pedersen, H. Ogasawara, A. Nilsson, S. Kaya, Interlayer Carbon Bond Formation Induced by Hydrogen Adsorption in Few-Layer Supported Graphene, Phys. Rev. Lett. 111 (2013) 085503. https://doi.org/10.1103/PhysRevLett.111.085503.

[11] F. Ke, L. Zhang, Y. Chen, K. Yin, C. Wang, Y.-K. Tzeng, Y. Lin, H. Dong, Z. Liu, J.S. Tse, W.L. Mao, J. Wu, B. Chen, Synthesis of Atomically Thin Hexagonal Diamond with Compression, Nano Lett. 20 (2020) 5916. https://doi.org/10.1021/acs.nanolett.0c01872.

[12] F. Piazza, K. Cruz, M. Monthioux, P. Puech, I. Gerber, Raman Evidence for the Successful Synthesis of Diamane, Carbon 169 (2020) 129. https://doi.org/10.1016/j.carbon.2020.07.068.

[13] B. Mortazavi, F. Shojaei, B. Javvaji, M. Azizi, H. Zhan, T. Rabczuk, X. Zhuang, First-Principles Investigation of Mechanical, Electronic and Optical Properties of H-, F- and Cl-Diamane, Appl. Surf. Sci. 528 (2020) 147035. https://doi.org/10.1016/j.apsusc.2020.147035.

[14] M. Raeisi, B. Mortazavi, E.V. Podryabinkin, F. Shojaei, X. Zhuang, A.V. Shapeev, High Thermal Conductivity in Semiconducting Janus and Non-Janus Diamanes, Carbon 167 (2020) 51. https://doi.org/10.1016/j.carbon.2020.06.007.

[15] O. Ruff, O. Bretschneider, Die Reaktionsprodukte der verschiedenen Kohlenstoffformen mit Fluor II (Kohlenstoff-monofluorid), Z. Anorg. Allg. Chem. 217 (1934) 1. https://doi.org/10.1002/zaac.19342170102.

[16] T. Nakajima, Fluorine-Carbon and Fluorine-Carbon Materials, Marcel Dekker, Inc., New York, 1995.

[17] Y. Kita, N. Watanabe, Y. Fujii, Chemical Composition and Crystal Structure of Graphite Fluoride, J. Am. Chem. Soc. 101 (1979) 3832. https://doi.org/10.1021/ja00508a020.

[18] N. Watanabe, Two Types of Graphite Fluorides, $(CF)_n$ and $(C_2F)_n$, and Discharge Characteristics and Mechanisms of Electrodes of $(CF)_n$ and $(C_2F)_n$ in Lithium Batteries, Solid State Ion. 1 (1980) 87. https://doi.org/10.1016/0167-2738(80)90025-9.

[19] H. Touhara, K. Kadono, Y. Fujii, N. Watanabe, On the Structure of Graphite Fluoride, Z. Anorg. Allg. Chem. 544 (1987) 7. https://doi.org/10.1002/zaac.19875440102.

[20] A. Tuteja, W. Choi, M. Ma, J.M. Mabry, S.A. Mazzella, G.C. Rutledge, G.H. McKinley, R.E. Cohen, Designing Superoleophobic Surfaces, Science 318 (2007) 1618. https://doi.org/10.1126/science.1148326.

[21] Y. Hernandez, V. Nicolosi, M. Lotya, F.M. Blighe, Z. Sun, S. De, I.T. McGovern, B. Holland, M. Byrne, Y.K. Gun'ko, J.J. Boland, P. Niraj, G. Duesberg, S. Krishnamurthy, R. Goodhue, J. Hutchison, V. Scardaci, A.C. Ferrari, J.N. Coleman, High-Yield Production of Graphene by Liquid-Phase Exfoliation of Graphite, Nature Nanotechnol. 3 (2008) 563–568. https://doi.org/10.1038/nnano.2008.215.

[22] X. Chen, J.F. Dobson, C.L. Raston, Vortex Fluidic Exfoliation of Graphite and Boron Nitride, Chem. Commun. 48 (2012) 3703. https://doi.org/10.1039/C2CC17611D.

[23] X. Chen, R.A. Boulos, P.K. Eggers, C.L. Raston, *p*-Phosphonic Acid Calix[8]arene Assisted Exfoliation and Stabilization of 2D Materials in Water, Chem. Commun. 48 (2012) 11407. https://doi.org/10.1039/C2CC36268F.

[24] J.R. Brent, N. Savjani, E.A. Lewis, S.J. Haigh, D.J. Lewis, P. O'Brien, Production of Few-Layer Phosphorene by Liquid Exfoliation of Black Phosphorus, Chem. Commun. 50 (2014) 13338. https://doi.org/10.1039/C4CC05752J.

[25] R. Zbořil, F. Karlický, A.B. Bourlinos, T.A. Steriotis, A.K. Stubos, V. Georgakilas, K. Šafářová, D. Jančík, C. Trapalis, M. Otyepka, Graphene Fluoride: A Stable Stoichiometric Graphene Derivative and its Chemical Conversion to Graphene, Small 6 (2010) 2885. https://doi.org/10.1002/smll.201001401.

[26] Y. Yang, G. Lu, Y. Li, Z. Liu, X. Huang, One-Step Preparation of Fluorographene: A Highly Efficient, Low-Cost, and Large-Scale Approach of Exfoliating Fluorographite, ACS Appl. Mater. Interfaces 5 (2013) 13478. https://doi.org/10.1021/am405046u.

[27] M. Zhang, L. Liu, T. He, G. Wu, P. Chen, Melamine Assisted Solid Exfoliation Approach for the Synthesis of Few-Layered Fluorinated Graphene Nanosheets, Mater. Lett. 171 (2016) 191. https://doi.org/10.1016/j.matlet.2016.02.042.

[28] L. Liu, M. Zhang, Z. Xiong, D. Hu, G. Wu, P. Chen, Ammonia Borane Assisted Solid Exfoliation of Graphite Fluoride for Facile Preparation of Fluorinated Graphene Nanosheets, Carbon 81 (2015) 702. https://doi.org/10.1016/j.carbon.2014.10.008.

[29] M. Dubois, K. Guérin, Y. Ahmad, N. Batisse, M. Mar, L. Frezet, W. Hourani, J. Bubendorff, J. Parmentier, S. Hajjar-Garreau, L. Simon, Thermal Exfoliation of Fluorinated Graphite, Carbon 77 (2014) 688. https://doi.org/10.1016/j.carbon.2014.05.074.

[30] M. Herraiz, M. Dubois, N. Batisse, S. Hajiar-Garreau, L. Simon, Large-Scale Synthesis of Fluorinated Graphene by Rapid Thermal Exfoliation of Highly Fluorinated Graphite, Dalton Trans. 47 (2018) 4596. https://doi.org/10.1039/C7DT04565D.

[31] S. Wu, J. Mo, Y. Zeng, Y. Wang, A. Rawal, J. Scott, Z. Su, W. Ren, S. Chen, K. Wang, W. Chen, Y. Zhang, C. Zhao, X. Chen, Shock Exfoliation of Graphene Fluoride in Microwave, Small (2019) 1903397. https://doi.org/10.1002/smll.201903397.

[32] W. Feng, P. Long, Y. Feng, Y. Li, Two-Dimensional Fluorinated Graphene: Synthesis, Structures, Properties and Applications, Adv. Sci. 3 (2016) 1500413. https://doi.org/10.1002/advs.201500413.

[33] D. Massiot, F Fayon, M. Capron, I. King, S. Le Calvé, B. Alonso, J.O. Durand, B. Bujoli, Z. Gan, G. Hoatson, Modelling One- and Two-Dimensional Solid-State NMR Spectra, Magn. Reson. Chem. 40 (2002) 70. https://doi.org/10.1002/mrc.984.

[34] G. Kresse, J. Furthmüller, Efficiency of ab-initio Total Energy Calculations for Metals and Semiconductors Using a Plane-Wave Basis Set, Comput. Mater. Sci. 6 (1996) 15-50. https://doi.org/10.1016/0927-0256(96)00008-0.

[35] G. Kresse, J. Furthmüller, Efficient Iterative Schemes for ab initio Total-Energy Calculations Using a Plane-Wave Basis Set, Phys. Rev. B 54 (1996) 11169–11186. https://doi.org/10.1103/PhysRevB.54.11169.

[36] J.P. Perdew, A. Ruzsinszky, G.I. Csonka, O.A. Vydrov, G.E. Scuseria, L.A. Constantin, X. Zhou, K. Burke, Restoring the Density-Gradient Expansion for Exchange in Solids and Surfaces, Phys. Rev. Lett. 100 (2008) 13. https://doi.org/10.1103/PhysRevLett.100.136406.

[37] J.P. Perdew, K. Burke, M. Ernzerhof, Generalized Gradient Approximation Made Simple, Phys. Rev. Lett. 77 (1996) 3865–3868. https://doi.org/10.1103/PhysRevLett.77.3865.

[38] L. Vannucci, U. Petralanda1, A. Rasmussen, T. Olsen, K.S. Thygesen, Anisotropic Properties of Monolayer 2D Materials: An Overview from the C2DB Database, J. Appl. Phys. 128 (2020) 105101. https://doi.org/10.1063/5.0021237.

[39] A. Togo, I. Tanaka, First Principles Phonon Calculations in Materials Science, Scr. Mater. 108 (2015) 1–5. https://doi.org/10.1016/j.scriptamat.2015.07.021.

[40] K. Momma, F. Izumi, VESTA 3 for Three-Dimensional Visualization of Crystal, Volumetric and Morphology Data, J. Appl. Crystallography 44 (2011) 1272–1276. https://doi.org/10.1107/S0021889811038970.

[41] R.F.W. Bader, Atoms in Molecules: A Quantum Theory. Oxford, New York: Oxford University Press, 1994.

[42] A. Otero-de-la-Roza, E.R. Johnson, V. Luaña, Critic2: A Program for Real-Space Analysis of Quantum Chemical Interactions in Solids, Comput. Phys. Commun. 185 (2014) 1007–1018. https://doi.org/10.1016/j.cpc.2013.10.026.

[43] L. Köhler, G. Kresse, Density Functional Study of CO on Rh(111), Phys. Rev. B 70 (2004) 165405. https://doi.org/10.1103/PhysRevB.70.165405.

[44] B. Wang, J. Wang, J. Zhu, Fluorination of Graphene: A Spectroscopic and Microscopic Study, ACS Nano 8 (2014) 1862. https://doi.org/10.1021/nn406333f.

[45] V. Gupta, T. Nakajima, B. Žemva, Raman Scattering Study of Highly Fluorinated Graphite, J. Fluor. Chem. 110 (2001) 145. https://doi.org/10.1016/S0022-1139(01)00422-5.

[46] W. Rüdorff, K. Brodersen, IR-Spektrum des Kohlenstoffmonofluorids, Z. Naturforsch. B 12 (1957) 595. https://doi.org/10.1515/znb-1957-8-923.

[47] R.J. Lagow, R.B. Badachhape, J.L. Wood, J.L. Margrave, Some New Synthetic Approaches to Graphite–Fluorine Chemistry, J. Chem. Soc., Dalton Trans. (1974) 1268. https://doi.org/10.1039/DT9740001268.

[48] W. Zhang, M. Dubois, K. Guérin, A. Hamwi, J. Giraudet, F. Masin, Solid-State NMR and EPR Study of Fluorinated Carbon Nanofibers, J. Solid State Chem. 181 (2008) 1915. https://doi.org/10.1016/j.jssc.2008.03.037.

[49] M. Dubois, J. Giraudet, K. Guérin, A. Hamwi, Z. Fawal, P. Piotte, F. Masin, EPR and Solid-State NMR Studies of Poly(dicarbon monofluoride) $(C_2F)_n$, J. Phys. Chem. B 110 (2006) 11800. https://doi.org/10.1021/jp061291m.

[50] M. Herraiz, N. Batisse, M. Dubois, V.V. Nesvizhevsky, C. Cavallari, M. Brunelli, V. Pischedda, S. Radescu, A Multitechnique Study of Fluorinated Nanodiamonds for Low-Energy Neutron Physics Applications, J. Phys. Chem. C 124 (2020) 14229. https://doi.org/10.1021/acs.jpcc.0c03083.

[51] C. Cavallari, M. Brunelli, S. Radescu, M. Dubois, N. Batisse, G.B.M. Vaughan, H.E. Fischer, V. Pischedda, Structural and Electronic Changes in Graphite Fluorides as A Function of Fluorination Rate: An XRS, PDF and DFT Study, Carbon 147 (2019) 1. https://doi.org/10.1016/j.carbon.2019.02.053.

[52] K. Yoshida, Y. Sugawara, M. Saitoh, K. Matsumoto, R. Hagiwara, Y. Matsuo, A. Kuwabara, Y. Ukyo, Y. Ikuhara, Microscopic Characterization of the C–F Bonds in Fluorine–Graphite Intercalation Compounds, J. Power Sources 445 (2020) 227320. https://doi.org/10.1016/j.jpowsour.2019.227320.

[53] C. Cavallari, S. Radescu, M. Dubois, N. Batisse, H. Diaf, V. Pischedda, Tuning C–F Bonding of Graphite Fluoride by Applying High Pressure: Experimental and Theoretical Study, J. Phys. Chem. C (in press) https://doi.org/10.1021/acs.jpcc.0c06860.

Graphical Abstract

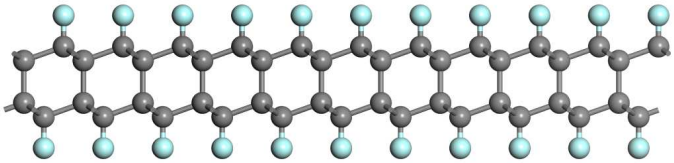

Keywords: diamane, graphite fluoride, fluorination, exfoliation, 2D materials